

Imaging of muscle activity-induced morphometric changes in fibril network of myofascia by two-photon microscopy

Chayanit Chaweewannakorn^{1,2} | Takashi Harada³ | Mazvita R. Nyasha² |
Masashi Koide³ | Yosuke Shikama⁴ | Yoshihiro Hagiwara³ | Keiichi Sasaki¹ |
Makoto Kanzaki²  | Masahiro Tsuchiya⁵ 

¹Division of Advanced Prosthetic Dentistry, Graduate School of Dentistry, Tohoku University, Sendai, Japan

²Graduate School of Biomedical Engineering, Tohoku University, Sendai, Japan

³Department of Orthopaedic Surgery, Graduate School of Medicine, Tohoku University, Sendai, Japan

⁴Department of Oral Disease Research, National Center for Geriatrics and Gerontology, Obu, Japan

⁵Department of Nursing, Tohoku Fukushi University, Sendai, Japan

Correspondence

Masahiro Tsuchiya, Department of Nursing, Tohoku Fukushi University, 6-149-1 Kunimi-ga-oka, Sendai 981-3201, Japan.
Email: tsuchiya-thk@umin.ac.jp

Funding information

Japan Society for the Promotion of Science

Abstract

Myofascia, deep fascia enveloping skeletal muscles, consists of abundant collagen and elastin fibres that play a key role in the transmission of muscular forces. However, understanding of biomechanical dynamics in myofascia remains very limited due to less quantitative and relevant approaches for in vivo examination. The purpose of this study was to evaluate the myofascial fibril structure by means of a quantitative approach using two-photon microscopy (TPM) imaging in combination with intravital staining of Evans blue dye (EBD), a far-red fluorescence dye, which potentially labels elastin. With focus on myofascia of the tibial anterior (TA) muscle, the fibril structure intravitaly stained with EBD was observed at the depth level of collagen fibrous membrane above the muscle belly. The EBD-labelled fibril structure and orientation in myofascia indicated biomechanical responses to muscle activity and ageing. The orientation histograms of EBD-labelled fibrils were significantly modified depending upon the intensity of muscle activity and ageing. Moreover, the density of EBD-labelled fibrils in myofascia decreased with habitual exercise but increased with muscle immobilization or ageing. In particular, the diameter of EBD-labelled fibrils in aged mice was significantly higher. The orientation histograms of EBD-labelled fibrils after habitual exercise, muscle immobilization and ageing showed significant differences compared to control. Indeed, the histograms in bilateral TA myofascia of exercise mice made simple waveforms without multiple sharp peaks, whilst muscular immobilization or ageing significantly shifted a histogram with sustaining multiple sharp peaks. Therefore, the dynamics of fibre network with EBD fluorescence in response to the biomechanical environment possibly indicate functional tissue adaptation in myofascia. Furthermore, on the basis of the knowledge that neutrophil recruitment occurs locally in working muscles, we suggested the unique reconstruction mechanism involving neutrophilic elastase in the myofascial fibril structure. In addition to the elastolytic susceptibility of EBD-labelled fibrils, distinct immunoreactivities and activities of neutrophil elastase in the myofascia were observed after electric pulse stimulation-induced muscle contraction for 15 min. Our findings of EBD-labelled fibril dynamics in myofascia through quantitative approach using

TPM imaging and intravital fluorescence labelling potentially brings new insights to examine muscle physiology and pathology.

KEYWORDS

aging, elastin, multi-photon microscopy, muscular activity, myofascia, neutrophil elastase

1 | INTRODUCTION

Myofascia is a type of connective tissue consisting of abundant extracellular matrix proteins, such as collagen and elastin fibres, and is also known as deep fascia that envelops skeletal muscles (Federative Committee on Anatomical Terminology, 1998; Marieb & Hoehn, 2007; McLoon et al., 2018). Elastic fibres interwoven with collagen bundles in myofascia provide dual properties to the peripheral tissues, viz. connectivity to retain the location and/or the flexibility to reduce friction during muscular contraction (Curran et al., 2008; McLoon et al., 2018). Myofascia plays a key role in the transmission of muscular forces with complicated distribution of tensile/compressive strain (Curran et al., 2008). Thus, the fibrous components of myofascia have been recognized to suffer potential injuries owing to muscular overuse or overloading (Chi et al., 2010; Curran et al., 2008; Tozzi, 2014). Myofascial constriction, a major sign in a chronic musculoskeletal pain disorder, such as myofascial pain syndrome (MPS), is a concept that concerns damage accumulation leading to local ischemia and inflammation in skeletal muscle tissues (Behm & Wilke, 2019; Krause et al., 2016). However, although there is significant clinical interest in the functional structure of myofascia, the understanding of biomechanical dynamics remains very limited due to less quantitative and relevant approaches for *in vivo* examination.

Two-photon microscopy (TPM) could reveal the detailed ultra-structures of connective tissues, including elastin and collagen fibres (>1.5 mm thick), with high three-dimensional (3D) resolution (Kawakami et al., 2015; Zoumi et al., 2004). Moreover, collagen fibres in mammalian soft tissues can be selectively visualized *in situ* by second harmonic generation (SHG) without staining (Servin-Vences et al., 2019; Zoumi et al., 2004). Reed et al. (2019) also recently reported quantitative destruction of collagen fibre in temporomandibular joint osteoarthritis using SHG imaging in combination with automated software analysis. Meanwhile, in terms of elastin imaging, a lot of studies have used autofluorescence signal to track the fibre structure, but few studies have been designed to explore the morphological quantification because of the difficulties in distinguishing the fibre types in complex connective tissues. Although there are limitations of TPM imaging using autofluorescence, Jun et al. (2017) demonstrated less image contrast with deeper target depth and suggested the significance of using far-red fluorescence dyes. Interestingly, several studies have reported that Evans blue dye (EBD), a bright far-red fluorescence dye used for intravital staining, characteristically binds with higher affinity to elastic fibrils in connective tissue owing to tissue microcirculation (Heinle & Lindner, 1984; Murphy & Lever, 2002; Weizsacker et al., 2014). Thus,

intravital staining with EBD potentially allows selective fluorescence visualization of the myofascial fibril structure.

Elastic fibrils consisting of elastin, the main component in myofascia, support the extensibility and flexibility of muscle dynamics (Federative Committee on Anatomical Terminology, 1998; Keeley et al., 2002; Yanagisawa & Wagenseil, 2019), and the fibre network can handle mechanical strain caused by muscle contraction with rearrangement in terms of orientation and attachment to other fibres (Ishihara et al., 2002; Montes, 1996; Pasquali-Ronchetti et al., 1995). The remodelling and/or turnover in connective tissues is modulated by several cell types, including immune cells producing growth factors, cytokines and various enzymes for extracellular matrix (Abraham et al., 2005; Mackey & Kjaer, 2017). Recently, employing physiological muscle activities (i.e. walking, mastication and muscle contraction) caused by low-intensity electrical stimulation, we demonstrated that neutrophils significantly migrate into skeletal muscle tissues during exercise and this influx supports muscular activity via promotion of metabolic incorporation (Chiba et al., 2015; Tsuchiya et al., 2018). In our hypothesis, local recruitment of neutrophils in working muscle after exercise triggers fibre remodelling of myofascia, leading to tissue adaptation for biomechanical advantages (Ferraro et al., 2014; Franchi et al., 2017; Ishihara et al., 2002). Fibre remodelling is due to the production of neutrophil elastase (ELANE), a major elastolytic enzyme with substrate specificity (Crocetti et al., 2019). However, there are far less studies available to demonstrate the role of neutrophil recruitment and enzyme secretion in order to contribute to myofascial remodelling post-exercise.

Therefore, in combination with TPM imaging and intravital staining using EBD, the purpose of this study was to quantitatively evaluate the ultra-structure of myofascial fibrils. We also clarified whether muscular activity plays a key role in maintaining the fibril network with local elastolytic enzymes secreted from neutrophils. Our results demonstrated the importance of exercise associated with a unique myofascial reconstruction system centred around neutrophils.

2 | METHODS

2.1 | Experimental animals

Young male (8–10-week-old) C57BL/6 mice weighing 27–30 g, purchased from CLEA-Japan, were used for muscle sample preparation. Aged male (2-year-old) C57BL/6 mice were provided by the National Center for Geriatrics and Gerontology. The experimental design, care and use of the mice were performed following the guidelines for

animal experiments of Tohoku University and the Ethics Committee for Animal Experiments, and Tohoku University approved these studies (2014Dna-020, 2017Dna-009). The mice were kept in standard cages maintained in an air-conditioned room at $23^{\circ}\text{C} \pm 1^{\circ}\text{C}$ with a 12-h light-dark cycle with ad libitum access to standard food pellets and tap water. For anaesthetization, mice were intraperitoneally injected with a mixture of medetomidine hydrochloride (0.3 mg/kg; ZENOAQ), midazolam (4.0 mg/kg; SANDZ), and butorphanol (5.0 mg/kg; Meiji Seika Pharma Co) before operation and during *in vivo* imaging.

2.2 | Intravital staining and muscle sample preparation

Mice were intravenously injected via the tail vein (*i.v.*) with 200 μl of intravital dyes in saline, including 0.5% EBD (Wako Pure Chemical Industries) at final concentration (Matsuda et al., 1995). After dye injection for 4–6 h, mice were sacrificed by cervical dislocation under inhalation anaesthesia with isoflurane (MSD Animal Health), and the dissected tibialis anterior (TA) muscles were immersed in 4% paraformaldehyde (PFA)/phosphate buffer for fixation before TPM imaging. It should be mentioned that according to the report by Heinle and Lindner (1984), we did not add any surfactants in the experimental buffers for preventing dye stripping from tissues with EBD intravital staining.

2.3 | TPM imaging

Imaging systems with non-linear optics, including TPM and SHG imaging, have been popular methods for the observation of deep tissue and intravital biological imaging. An upright A1R-MP multiphoton microscope (Nikon) equipped with a Ti-sapphire laser (Mai-Tai DeepSee, Spectra-Physics), GaAsP non-descanned detectors, and a water-immersion objective lens (CFP75 Apo LWD 25x/NA1.1) was used for image recording with excitation laser consistently set at 920 nm, area size 0.25 μm by 0.25 μm and a resolution of 600 dpi. A high resolution galvano scanner was consistently used, and a resonant scanner was used only in the time-lapse experiments for high acquisition speed during live imaging. The wavelengths for detection using emission filter cubes were 492/SP nm for SHG signals (blue channel) and 629 ± 56 nm for EBD (far-red channel), respectively. From the entire data of sequential images in muscle structure, representative 3D image stacks focusing on EBD-labelled fibrils and collagenous deep membrane in myofascia were reconstructed with Fiji software (NIH). TA muscles were placed straight on the microscope stage along the direction of muscle bundles to keep the ankle tendon downwards during the whole imaging process, and 8–10 images from each TA muscle were randomly obtained from a wide field. For *in vivo* imaging (Figure 2), after skin incision, the anaesthetized mouse was mounted on a home-made holder with the temperature set at 28°C to preserve mouse body temperature before EBD injection. TPM imaging of the live TA muscle was obtained at the same point every 30 min until 4 h before and after EBD injection.

2.4 | Quantification of myofascial fibril structure from TPM and SHG imaging

The captured TPM images were analysed by DiameterJ for Fiji software (NIH), an open and validated tool, to determine fibril structural characteristics, such as length and intersection density of EBD-labelled fibrils (Hotaling et al., 2015). In brief, the original images were converted to binary images using Otsu's automatic thresholding method, and the setting values of minimum and maximum radius were set at 0.25–5 μm , as determined by our preliminary measurements. After automatic data processing, including considering the data to create histograms of EBD-labelled fibril orientation, visual directional analysis using the captured representative TPM images was also performed with Gaussian gradient in DiameterJ (Hotaling et al., 2015; Puspoki et al., 2016; Rezakhaniha et al., 2012).

2.5 | Habitual voluntary wheel running

The mice were kept in standard cages equipped with a free-wheel running apparatus (#ENV-047, Med Associates, Inc.) for monitoring the exercise behaviour for 4 weeks (Goh & Ladiges, 2015). Mice housed in standard cages without access to voluntary wheel running were used as sedentary controls.

2.6 | Unilateral hindlimb immobilization

Under anaesthetization, surgical skin staples (Precise Vista Lite; 3M) were attached to the unilateral hindlimb (right side) in dorsotibial flexion to immobilize the muscle so as to render it as disused muscle (Caron et al., 2009). The other limb was left intact, and intact hindlimbs from mice without immobilization were used as control (Cont) to avoid artificial errors from overload. After 7 days of immobilization, mice were injected with intravital dyes and proceeded for muscle collection.

2.7 | Electrical muscle contractions (EPS) and immunohistochemistry (IHC)

Mice hindlimb was exposed by a skin incision over the TA region, and two needle electrodes (tip diameter, 0.08 mm; conductive tip exposure, 1.5 mm, inter polar distance, ~10 mm) were inserted. The direct electric stimulation protocol was performed by electrical stimulation using an STG4004 stimulus generator (Multi Channel Systems) for inducing muscle contraction in the unilateral limb for 15 min (electrical pulse rate, 1/s; pulse rate, 50 Hz; duration, 1 ms at 2.5 mA), whereas the other limb remained as the control (Tsuchiya et al., 2018). TA tissues after PFA fixation and immersion in 30% sucrose solution were subjected to 4- μm thick cryosection for fluorescent IHC staining. The cryosections were blocked with 5% normal goat serum (NGS) and 1% bovine serum albumin (BSA) in phosphate buffered saline (PBS), followed by incubation with rabbit polyclonal anti-Elastase

(1:1000; #ab21593; Abcam) and rat anti-granulocyte-differentiation antigen 1 (Gr-1) antibody (1:500; RB6-8C5; BioLegend) in 5% NGS-PBS and counterstained with Alexa Fluor 488 donkey anti-rabbit, Alexa Fluor 555 donkey anti-rat (1:750; Invitrogen), and DAPI (4',6-diamidino-2-phenylindole; 1:1000; Dojindo) in 0.05% Triton X-PBS. The slides were examined under a fluorescence microscope (BZ-9000 BIOREVO, KEYENCE). The specificity of immune reactions was verified by replacing the primary antibody with rabbit IgG (#ab27472, Abcam) as an isotype control (Chiba et al., 2015).

2.8 | Elastase digestion of muscle tissues

After TPM imaging of TA intravitaly stained with EBD, the tissues were immersed in elastase collected from porcine pancreas (#E1250; Sigma-Aldrich), diluted in PBS at 0.5 mg/ml and incubated at 37°C for 4 h. Then, muscle tissues were washed with PBS to stop digestion and further subjected to TPM imaging.

2.9 | Neutrophil elastase activity assay

After 15 min of electrical stimulation, mice were rested for 30 min and then sacrificed by cervical dislocation. The dissected crural fascia on TA muscles was used for neutrophil elastase activity assay (#ab204730; Abcam), according to the manufacturer's instructions. Tissues were homogenized in lysis buffer containing 30 mM Tris-HCl and 100 mM NaCl. The lysate supernatant was incubated with neutrophil elastase substrate, and the fluorescence signal was then measured (excitation/emission = 380/500 nm) in a kinetic mode at 37°C for 20 min with a SpectraMax M5 Microplate Reader (Molecular Devices, MDS Analytical Technologies).

2.10 | Statistical analysis

Statistical analyses were performed using SPSS Statistics version 23 (IBM). All experimental data are presented as means \pm SE. Statistically significant differences were determined by the t-test or Kolmogorov-Smirnov test for normalized distribution of EBD-labelled fibril orientation. *p*-value of <0.05 indicated statistically significant difference.

3 | RESULTS

3.1 | Structural characteristics of TA myofascia in TPM imaging

First, in terms of multi-photon microscope settings during imaging, we consistently set the laser wavelength at 920 nm while changing the excitation laser wavelengths between 760–1040 nm (Figure S1). Indeed, autofluorescence itself is generally mentioned as the problem for quantitative histological analysis due to unstable

intensity (Clancy & Cauller, 1998; Pyon et al., 2019). Murphy and Lever interestingly reported autofluorescence of elastin fibrils in both green and far-red regions of the spectrum at the same levels, whereas EBD fluorescence was detected only in the far-red channel near 680 nm (Murphy & Lever, 2002). Thus, the applied laser power in TPM imaging was consistently set at a lower power level (0.8% of the total supplied laser power, approximately 1600 mW), which enabled detection of only EBD fluorescence in the far-red region but not of any fluorescence in the green region (Figure S2).

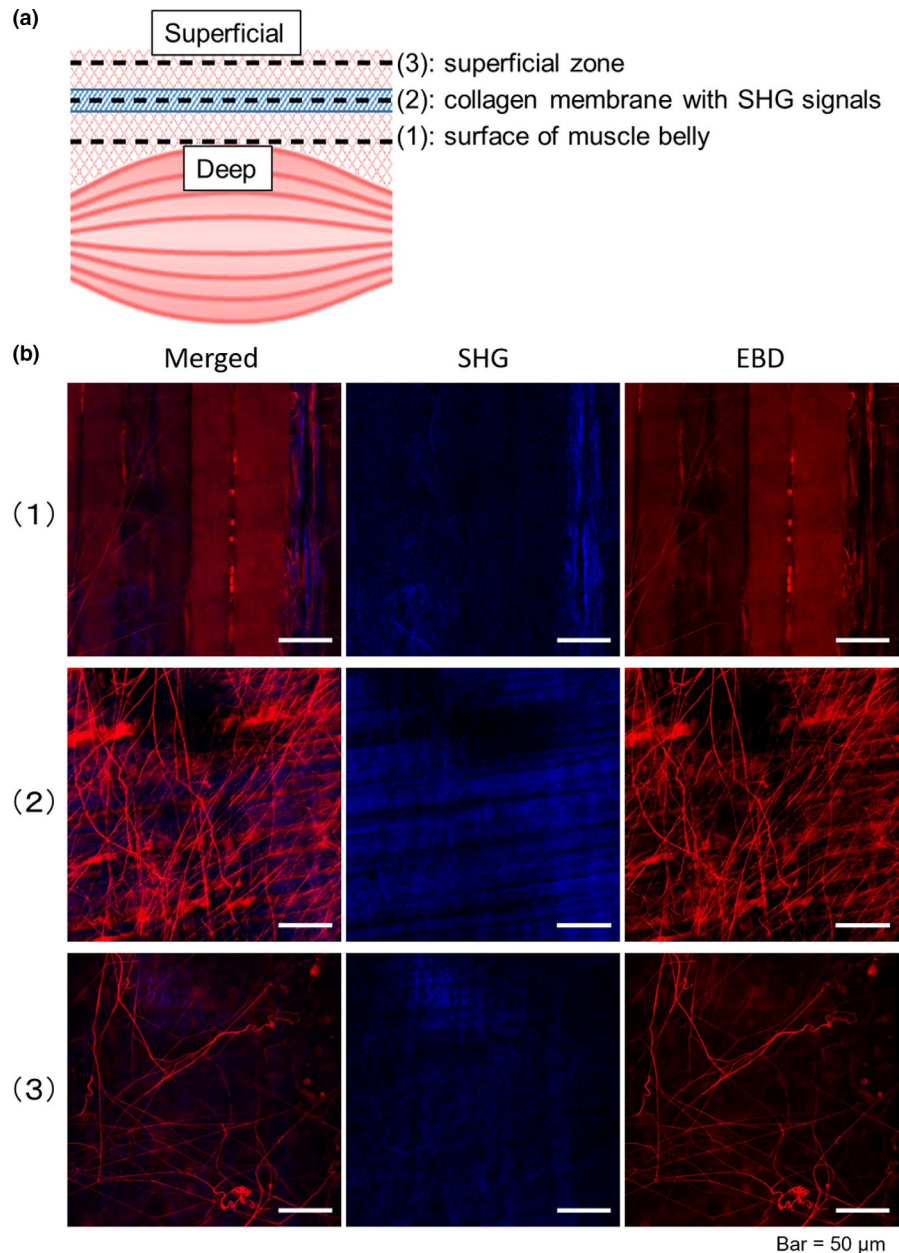
Utilizing the advantage of deep tissue penetration of TPM, we defined the structural orientation of TA myofascia intravitaly stained with EBD. The representative sequential and reconstruction images of 3D slices of TA myofascia are shown as supplemental data (Movies S1 and S2). As shown in Figure 1a (above), myofascia above the surface of TA muscle belly (Figure 1a, upper panels) involved collagen fibrous membrane recognized with SHG signal (Figure 1a, middle panels, blue) at approximately 35 μ m (mean \pm SE, 34.7 \pm 2.2 μ m; Figure S4a) from the muscle belly measured using the z-axis calculator in TPM apparatus. Interestingly, EBD-positive fibrils (mean diameter \pm SE: 0.346 \pm 0.001 μ m in control TA myofascia) were widely observed in the TA myofascia up to approximately 100 μ m above the muscle fibres (Figure 1a, lower panels), but the most distinct observations of EBD-labelled fibrils were obtained at the level of the collagen fibrous membrane with fibril insertions. Thus, to focus on the structural and dynamical aspects of EBD-positive fibrils in myofascia related to biomechanical loadings, the observational points to obtain TPM images were settled at the depth level of collagen fibrous membrane in the whole imaging process. It should be noted that EBD-positive fibrils were observed in other surface skeletal muscles, such as quadriceps femoris, triceps surae and masseter; however, the TA muscle was the focus in this current study due to its observable and representative features. In addition, TA has been popular in both exercise and immobilization experimental models (Caron et al., 2009; Ishihara et al., 2002; Tsuchiya et al., 2018).

3.2 | Dye penetration in myofascial fibril structure

Time-course observation before and after EBD injection indicated time-dependent accumulation of EBD fluorescence signals in the myofascial fibril structure (Figure 2). The intensity of EBD fluorescence signals in the myofascial fibril structure was not detectable around 30 min after EBD injection, and the fluorescence intensity slowly increased by 4 h. However, blood vessels in TA muscle tissues were detected within a few minutes after EBD injection and were distinctly distinguished from EBD-labelled fibrils due to the intravascular flow of erythrocytes and the higher diameter. The length density of EBD-labelled fibrils increased consistently, but the variation decreased with time after EBD injection (Figure 2b).

Intravital staining of connective tissues with EBD is reportedly dependent upon tissue microcirculation after the dye reaches the concerned tissue via the circulating system. Moreover, whole mount

FIGURE 1 Structural characteristics of fibrils in myofascia by TPM/SHG imaging. (a) Basic structural characteristics of TA myofascia and (b) representative TPM/SHG images (*lower panels*) after intravital staining with EBD (red). Collagen fibre/membrane recognized as a SHG signal (blue) are located at the level of approximately 35 μm on an average above the surface of TA muscle belly (*upper panels*). The highest density of EBD-labelled fibrils is observed around the collagen fibrous membrane (*middle panels*). EBD-labelled fibrils in myofascia are observed up to approximately 100 μm above (*lower panels*). EBD, Evans blue dye; SHG, secondary harmonic generation. Bar = 50 μm



staining could not identify myofascial fibrils with EBD fluorescence signals either with or without tissue fixation (Figure S3a), but intravital staining with intraperitoneal EBD injection showed EBD-labelled fibrils in TA myofascia similar to that observed with the i.v. method (Figure S3b).

3.3 | Decrease in EBD-labelled fibrils in myofascia after habitual exercise

The morphological dynamics of EBD-labelled fibrils in myofascia were examined after habitual exercise by a quantitative approach. Compared to the sedentary control group, voluntary habitual exercise for a month resulted in a decrease in EBD-labelled fibrils, particularly with a negative direction in myofascia (Figure 3a). It should

be noted that, however, the depth from collagen fibrous membrane to the surface of the muscle belly and the crossing angle between muscle and collagen fibres were not statistically changed with habitual exercise (Figure S4a and b). The mean diameter of EBD-labelled fibrils was not different, but the length and intersection density of EBD-labelled fibrils decreased significantly by three-quarter and half with habitual exercise, respectively (Figure 3b). The orientation histograms of EBD-labelled fibrils between sedentary control and exercise mice showed a significant difference ($p < 0.05$; Figure 3c). The orientation histogram of EBD-labelled fibril in TA myofascia of both hindlimbs in the sedentary control mice symmetrically included three sharp peaks at -45° , 0° and 45° (Figure S5), but the histogram in the exercise group showed a simple curve with a single higher peak at 45° in the right (Figure 3c) or at -45° in the left TA myofascia (Figure S4c).

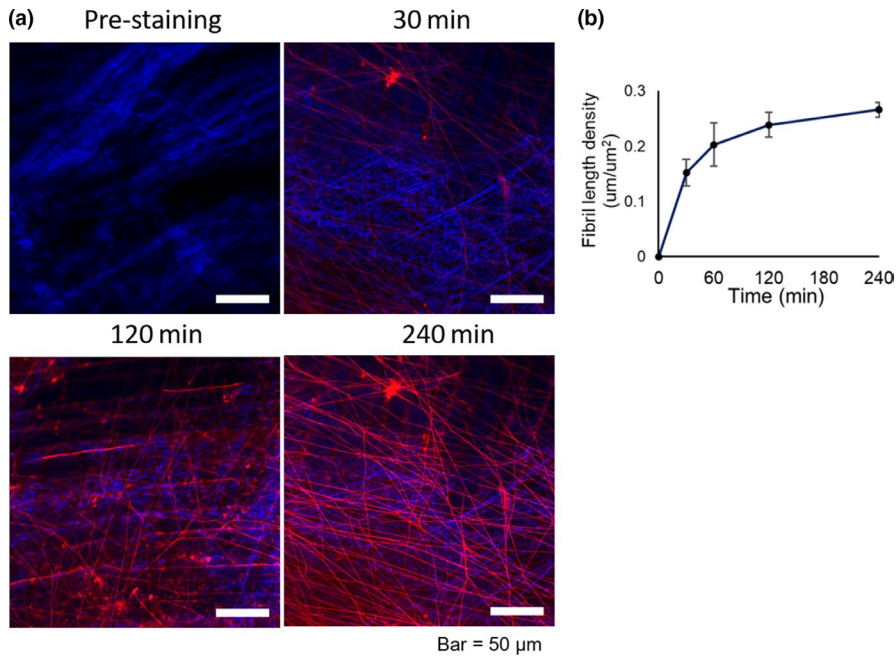


FIGURE 2 Dye penetration properties of EBD-labelled fibrils in TA myofascia. (a) Time-course images of TA tissues obtained before and after intravital staining with EBD for 30, 120, and 240 min. Similar results were obtained in three independent experiments. Bar = 50 μm . (b) Time-course changes in the length density of EBD-labelled fibrils. All data are shown as mean \pm SE

3.4 | Impact of immobilization on EBD-labelled fibril structures in myofascia

In disused model of TA, caused by immobilization of the ankle joint for a week, EBD-labelled fibrils in myofascia were also affected (Figure 4). Compared to the intact TA myofascia, the density of EBD-labelled fibrils in TA myofascia of the fixed-limb group was higher, and their angle orientation was slightly rotated right towards a positive direction (Figure 4a). Less muscular activity with hindlimb immobilization significantly increased the density of EBD-labelled fibrils (Figure 4b). The orientation histogram of EBD-labelled fibrils in TA myofascia was significantly different with the inclination towards a positive angle direction compared to that of the intact TA myofascia ($p < 0.01$; Figure 4c).

3.5 | Effects of ageing on EBD-labelled fibril structures in myofascia

To understand the physiological importance of ageing, we compared aged mice to young mice (aged 8–10 weeks). The EBD-labelled fibril structure in TA myofascia of aged mice was more distinct (Figure 5a), and the mean diameter of EBD-labelled fibrils in the aged group was significantly higher than that in the young group (Figure 5b, left). The density of EBD-labelled fibrils also increased significantly with ageing (Figure 5b), as observed in TA myofascia of immobilized mice. The orientation histogram of EBD-labelled fibrils showed a significant difference between aged and young mice ($p < 0.01$; Figure 5c). The angle distribution of EBD-labelled fibrils in TA myofascia of the right hindlimb in aged mice showed a more negative angle direction compared to that in the young group. It should be noted that because of

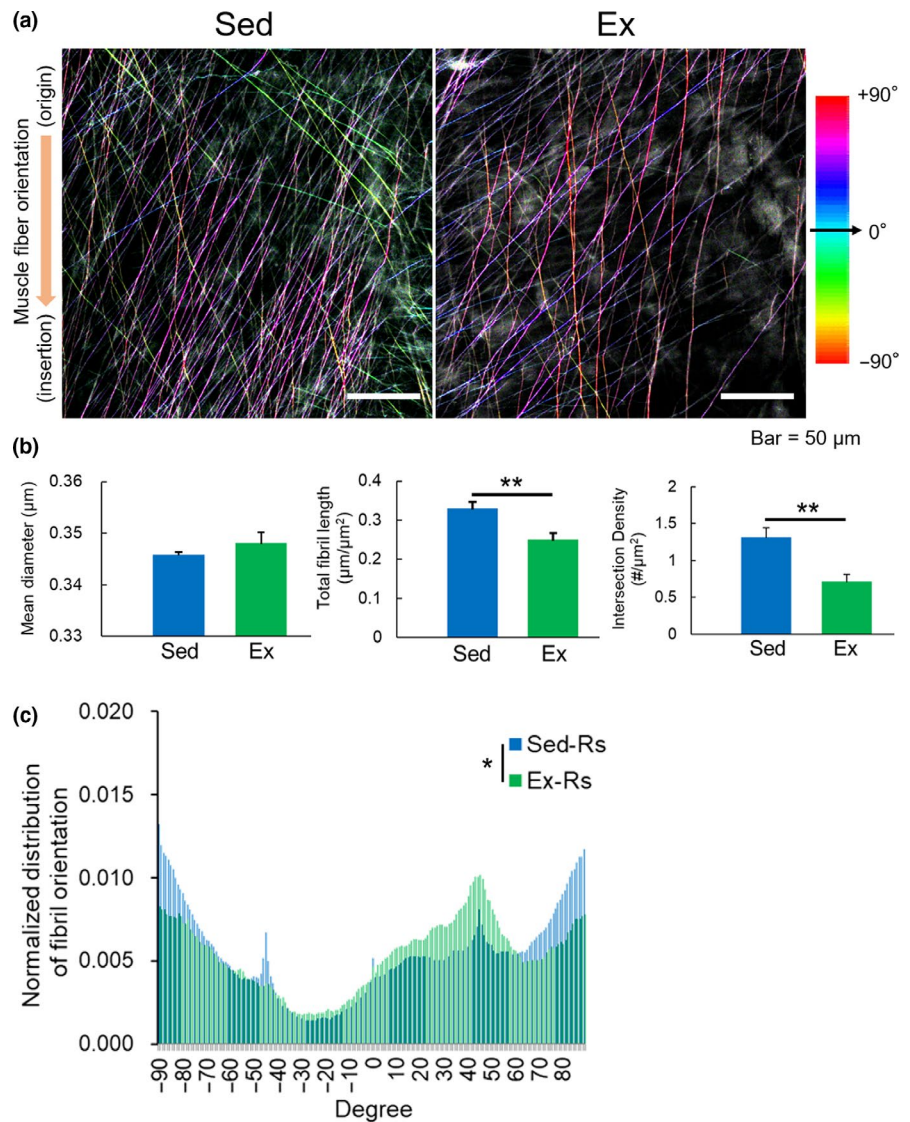
symmetry, the same trend was observed in the left hindlimb ($p < 0.001$; Figure S6).

3.6 | Possible involvement of neutrophil elastase in myofascial remodelling of fibril structure with muscle contraction

In order to clarify whether the fibril structure, intravitaly stained with EBD, primarily consists of elastin, we compared the EBD-labelled fibril structures before and after elastase digestion (Figure 6a). The EBD-labelled fibril structure in TA myofascia detected in TPM imaging decreased significantly post digestion of elastase (Figure 6b), but collagen fibres and membrane were clearly preserved after elastase digestion.

Next, we have recently revealed the supporting role of neutrophil recruitment in working muscles during muscular activity (Chiba et al., 2015; Tsuchiya et al., 2018). To investigate how elastolytic enzymes such as ELANE, a major specific elastase produced by neutrophils, possibly contributes to the remodelling of the elastic fibril structure in myofascia, we performed IHC analysis of ELANE. Although haematoxylin and eosin staining showed typical skeletal muscle tissue histology in both groups (data not shown), intense immunoreactivities of ELANE in TA myofascia were observed after 15 min of EPS-induced muscle contraction compared to that of TA myofascia in control mice (Figure 6c). Based on the increase of cells with immunoreactivities of Gr-1, a major neutrophil marker, ELANE-producing cells were mostly neutrophils (Figure 6c, lower panels). ELANE activity in homogenates of TA muscle tissues, including myofascia, was upregulated with EPS-induced muscle contraction (Figure 6d), corresponding with IHC observation. These results indicated that neutrophil infiltration after exercise may play a role

FIGURE 3 Effect of habitual exercise on EBD-labelled fibril structure and orientation in TA myofascia. (a) Representative TPM images of EBD-labelled fibrils in TA myofascia of control sedentary (Sed) and chronic voluntary wheel running (Ex) mice. Colour mapping code of fibril orientation preference is indicated. (b) Quantitative assessments of the mean diameter, length and intersection density, and (c) orientation histogram of EBD-labelled fibrils observed in myofascia of the right TA ($n = 6-8$). All data are shown as mean \pm SE and analysed using unpaired *t*-test or Kolmogorov-Smirnov test for distribution of fibril orientation. Statistical significance is indicated with * ($p < 0.05$) and ** ($p < 0.01$), respectively. Rs, right-side hindlimb



in contributing to the remodelling of the elastic fibril structure in myofascia via the production of elastolytic enzymes.

4 | DISCUSSION

With a combination of quantitative approach and intravital fluorescence staining of the myofascial fibril structure, the present study was designed to clarify whether the dynamics of the myofascial fibril structure, primarily consisting of elastin, are dependent upon muscular activity and ageing. Indeed, potentially favourable action of neutrophils locally recruited with muscle contraction was involved in maintaining muscle structure and strength via elastolytic activities.

Despite the growing focus on myofascia in view of muscular physiology and pathology, there has not been a validated and accessible approach with regard to quantitative analysis of myofascial fibrous structure. DiameterJ, an open application, enables researchers to quantitatively examine the myofascial fibril structure and could potentially provide new insights into the biomechanics of skeletal

muscles with future studies. Although future studies are warranted to clarify the association between elastin and the EBD-labelled fibril structures, our key finding using fluorescence-based contrast by EBD injection is that the fibril structure with elastolytic susceptibility in myofascia indicates biomechanical responses to muscle activity, i.e. the density of EBD-labelled fibrils in myofascia decreased with habitual exercise (Figure 3) but increased with muscle immobilization (Figure 4). The angle distribution of fibril orientation in myofascia would be a more sensitive indicator against biomechanical environment. The association of the fibril structure with muscular function remains unclear; however, habitual exercise definitively contributes in supporting and promoting roles for muscular activity, whereas immobilization leads to the disturbance of muscular structural function as a general consensus (Cohen et al., 2015; Theodorakopoulos et al., 2017). Furthermore, consistent with this notion from a clinical view, for patients with MPS, physical therapies including “myofascial release” have frequently been used for the improvement of muscular function for pain elimination with a shorter response time (Ajimsha et al., 2015; Behm & Wilke, 2019). Thus, further studies to clarify the

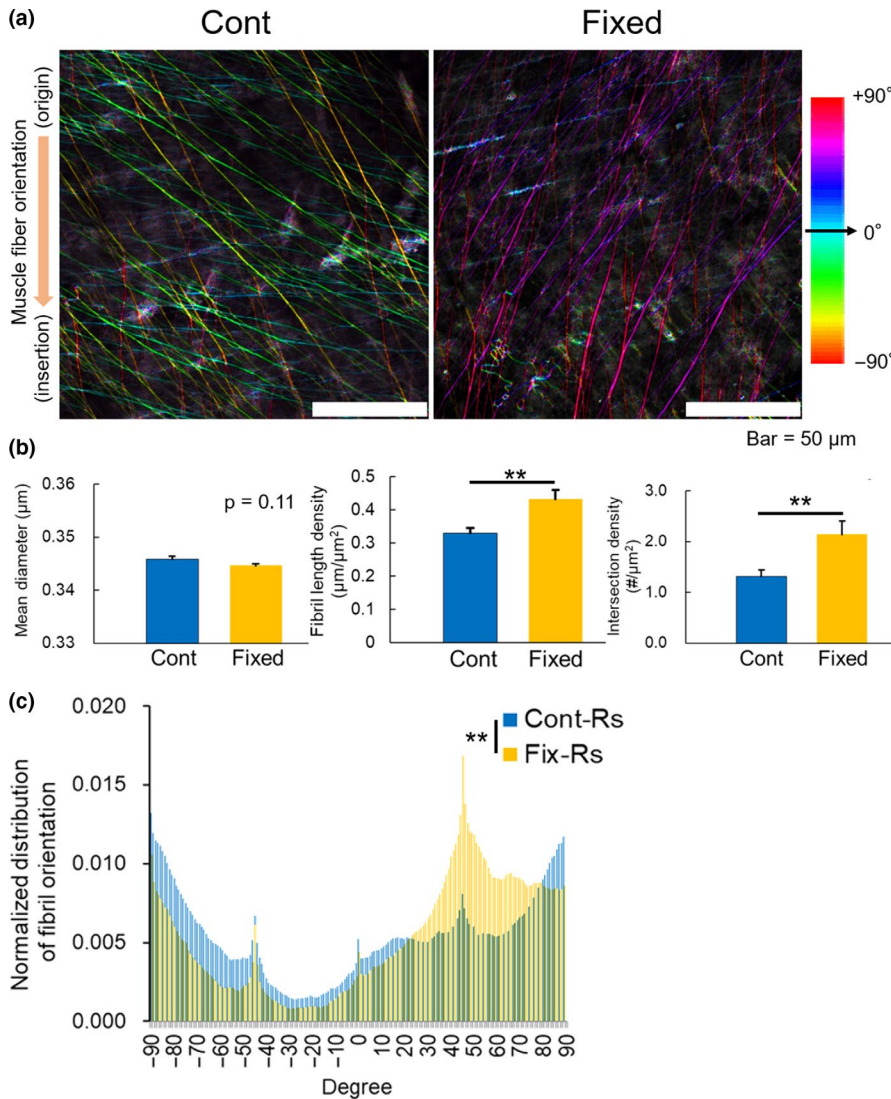


FIGURE 4 Impact of unilateral hindlimb immobilization on EBD-labelled fibril structure and orientation in TA myofascia. (a) Representative TPM images of EBD-labelled fibrils in myofascia of intact (Cont) and staple-immobilized TA (Fixed). Colour mapping code of fibril orientation preference is indicated. (b) Quantitative assessments of the mean diameter, length and intersection density, and (c) orientation histogram of EBD-labelled fibrils ($n = 6-8$). All data are shown as mean \pm SE and analysed using unpaired *t*-test or Kolmogorov-Smirnov test for distribution of fibril orientation. Statistical significance is indicated as ** ($p < 0.01$). Rs, right-side hindlimb

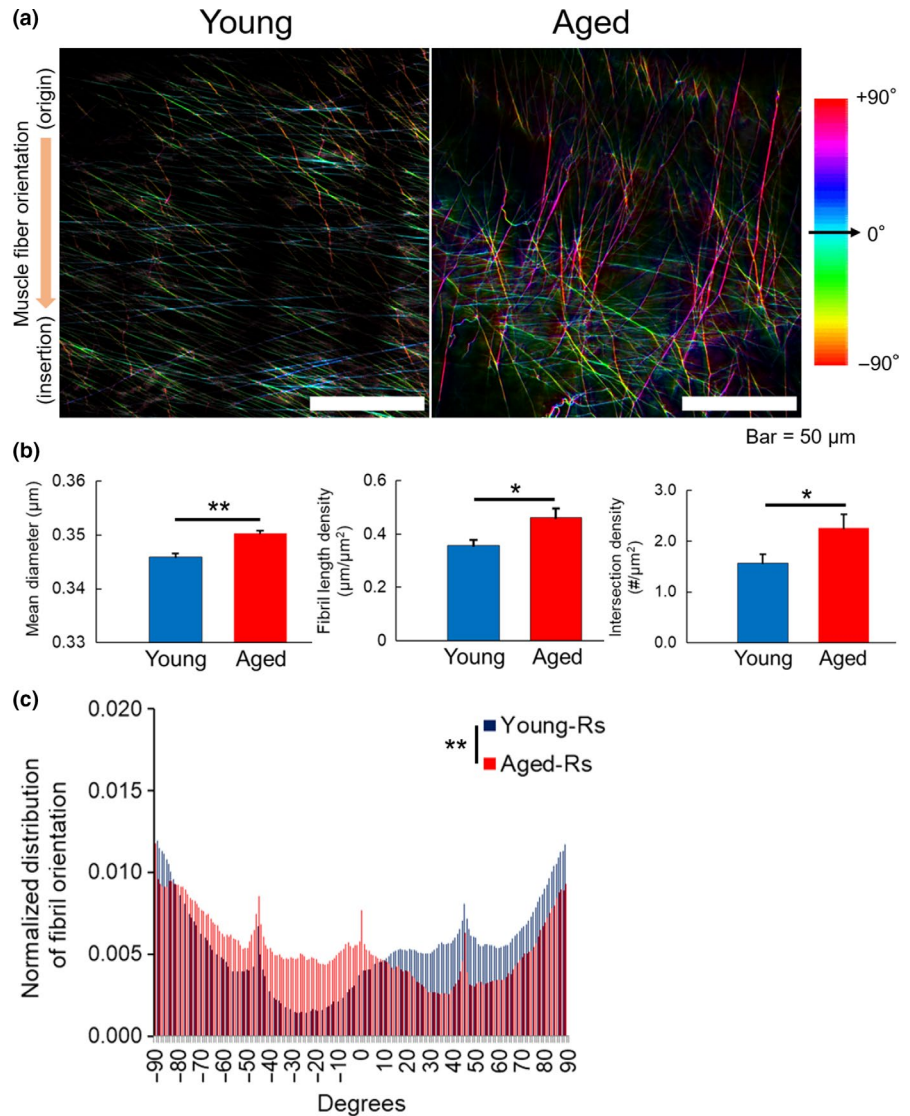
relationship between muscular function(s) and elastic fibril dynamics in myofascia are warranted.

In addition to the labelling characteristics of EBD described in previous studies (Heinle & Lindner, 1984; Murphy & Lever, 2002; Weizsacker et al., 2014), the results of elastolytic susceptibility also revealed a dominant elastin component in the myofascial fibril structure labelled with EBD (Figure 6a and b). Elastin is a major myofascial component responsible for maintaining muscle performance with force transmission, particularly during exercise (Keeley et al., 2002; Pasquali-Ronchetti et al., 1995; Yanagisawa & Wagenseil, 2019). In accordance with the rearrangement of elastic fibre network under mechanical loading (Montes, 1996), the dynamics of elastic fibrils in myofascia with muscle activity possibly include functional tissue adaptation. Several mouse exercise models (walking, chewing and EPS-induced muscle contraction) have shown that the increase of neutrophils in working skeletal muscles is a characteristic muscle contraction phenomenon (Neubauer et al., 2013; Phillips et al., 2000). We have demonstrated that neutrophil local recruitment

activates muscle performance due to the upregulation of muscle metabolism, thus, alleviating muscle fatigue (Chaweewannakorn et al., 2019; Chiba et al., 2015; Tsuchiya et al., 2018). Herein, as a new insight in muscle biology, neutrophilic elastase was observed to be potentially involved in biomechanical adaptation via the remodelling of elastic fibre network in myofascia. However, on the basis of anatomical knowledge that myofascia has less vessels (Federative Committee on Anatomical Terminology, 1998; Marieb & Hoehn, 2007), local migration of neutrophils producing ELANE would be the reasonable underlying mechanism of myofascial remodelling.

With respect to the angle distribution of fibril orientation in myofascia, three sharp peaks at -45° , 0° and 45° were generally observed but not after habitual exercise (Figure 3c). Furthermore, muscular immobilization transferred the angle distribution of EBD-labelled fibrils to a positive direction in the right TA myofascia (Figure 4c). However, interestingly, the right TA myofascia in aged mice showed angle distribution with a shift to a negative direction, unlike immobilized TA, and the diameter of fibrils

FIGURE 5 Effect of ageing on EBD-labelled fibril structure and orientation in TA myofascia. (a) Representative TPM images of EBD-labelled fibrils in TA myofascia of young (*left*) and aged mice (*right*). Colour mapping code of fibril orientation preference is indicated. (b) Quantitative assessments of the mean diameter, length, and intersection density, and (c) orientation histogram of EBD-labelled fibrils in the right TA myofascia ($n = 6-8$). All data are shown as mean \pm SE and analysed using unpaired *t*-test or Kolmogorov-Smirnov test for distribution of fibril orientation. Statistical significance is indicated as * ($p < 0.05$) and ** ($p < 0.01$), respectively. Rs, right-side hindlimb



increased. In skeletal muscle tissue of aged mice, mass decreases in association with less locomotor activity (Kadoguchi et al., 2019; Shoji & Miyakawa, 2019) and tissue turnover is further delayed (Svensson et al., 2016). Therefore, notwithstanding that more data points are necessary for analysis, the impact of ageing in the EBD-labelled fibril structure and orientation in myofascia must be observed. Although the observations would be typical only for TA myofascia, our results suggest that the quantitative approach of observing EBD-labelled fibrils in myofascia entails potentially several benefits to investigate muscular biology and pathology with new insights.

In summary, our findings of myofascial fibril dynamics advanced by the quantitative approach using TPM imaging and intravital fluorescence labelling using EBD provide new insights to examine muscle physiology and pathology. Although these methodological benefits are still confirmed only in animal experiments, clinical applicability will be analysed in the near future to establish a non-invasive approach via skin with improvement and development of microscopy and fluorescence dyes.

ACKNOWLEDGEMENTS

The authors are grateful to Dr. Hiroyasu Hatakeyama, Mr. Shigenori Sekiai and Ms. Natsumi Emoto at the Tohoku University Graduate School of Biomedical Engineering for her technical assistance. We thank Dr. Kazuki Iwata at Tohoku Fukushi University, Prof. Yoshitaka Kimura and Dr. Yoshiyuki Kasahara at the Department of Advanced Interdisciplinary Biomedical Engineering, Tohoku University Graduate School of Medicine, for their excellent technical advices with this study. This work was supported in part by grants from the Japan Society for the Promotion of Science (nos. 16K11580 and 19K10229 to M.T.).

CONFLICT OF INTEREST

No potential conflict of interest was reported by the authors.

AUTHOR CONTRIBUTIONS

Chayanit Chaweewannakorn, Takashi Harada, Masashi Koide and Masahiro Tsuchiya conducted the experiments. Yosuke Shikama, Yoshihiro Hagiwara and Keiichi Sasaki provided reagents/materials/analysis tools. Makoto Kanzaki and Masahiro Tsuchiya.

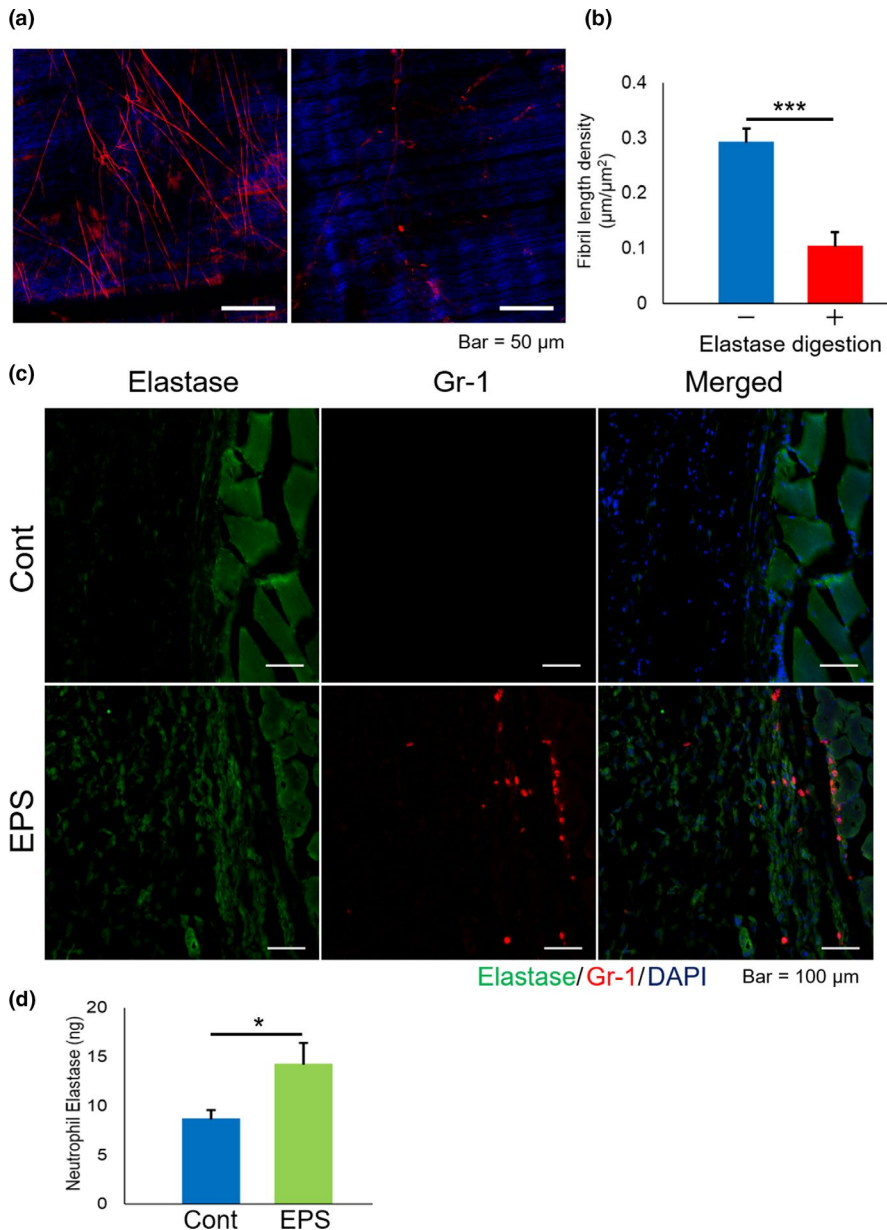


FIGURE 6 Elastolytic susceptibility of EBD-labelled fibrils and possible involvement of neutrophil elastase in fibril remodelling of myofascia. (a) Representative TPM images and (b) length density of EBD-labelled fibrils in TA myofascia before and after elastase digestion ($n = 6$). (c) Representative IHC images of mouse TA tissue with or without electrical pulse stimulation (EPS), indicating elastase (green), Gr-1 (red), and DAPI (blue). (d) Neutrophil elastase (ELANE) activity between control TA and EPS-treated TA. Data in graph are represented as mean \pm SE, and statistical significance was analysed with paired t -test, in which * and *** indicate $p < 0.05$ and < 0.001 , respectively

designed the experiments. Chayanit Chaweewannakorn, Mazvita R. Nyasha and Masahiro Tsuchiya wrote paper. All authors contributed to data analysis and extensively to the work presented in this paper.

ORCID

Makoto Kanzaki  <https://orcid.org/0000-0002-6884-2955>

Masahiro Tsuchiya  <https://orcid.org/0000-0002-7000-4547>

REFERENCES

- Abraham, S., Kumar, M.S., Sehgal, P.K., Nitish, S. & Jayakumar, N.D. (2005) Evaluation of the inhibitory effect of triphala on PMN-type matrix metalloproteinase (MMP-9). *Journal of Periodontology*, *76*, 497–502.
- Ajimsha, M.S., Al-Mudahka, N.R. & Al-Madzhar, J.A. (2015) Effectiveness of myofascial release: systematic review of randomized controlled trials. *Journal of Bodywork and Movement Therapies*, *19*, 102–112.
- Behm, D.G. & Wilke, J. (2019) Do self-myofascial release devices release myofascia? Rolling mechanisms: A narrative review. *Sports Medicine (Auckland, N. Z.)*, *49*, 1173–1181.
- Caron, A.Z., Drouin, G., Desrosiers, J., Trenz, F. & Grenier, G. (2009) A novel hindlimb immobilization procedure for studying skeletal muscle atrophy and recovery in mouse. *Journal of Applied Physiology*, *106*(6), 2049–2059.
- Chaweewannakorn, C., Nyasha, M.R., Chen, W., Sekiai, S., Tsuchiya, M., Hagiwara, Y. et al. (2019) Exercise-evoked intramuscular neutrophil-endothelial interactions support muscle performance and GLUT4 translocation: a mouse gnawing model study. *Journal of Physiology*, *598*(1), 101–122.
- Chi, S.W., Hodgson, J., Chen, J.S., Reggie Edgerton, V., Shin, D.D., Roiz, R.A. et al. (2010) Finite element modeling reveals complex strain mechanics in the aponeuroses of contracting skeletal muscle. *Journal of Biomechanics*, *43*, 1243–1250.
- Chiba, K., Tsuchiya, M., Koide, M., Hagiwara, Y., Sasaki, K., Hattori, Y. et al. (2015) Involvement of IL-1 in the maintenance of masseter muscle activity and glucose homeostasis. *PLoS One*, *10*, e0143635.

- Clancy, B. & Cauller, L.J. (1998) Reduction of background autofluorescence in brain sections following immersion in sodium borohydride. *Journal of Neuroscience Methods*, 83, 97–102.
- Cohen, S., Nathan, J.A. & Goldberg, A.L. (2015) Muscle wasting in disease: molecular mechanisms and promising therapies. *Nature Reviews Drug Discovery*, 14, 58–74.
- Crocetti, L., Quinn, M.T., Schepetkin, I.A. & Giovannoni, M.P. (2019) A patenting perspective on human neutrophil elastase (HNE) inhibitors (2014–2018) and their therapeutic applications. *Expert Opinion on Therapeutic Patents*, 29, 555–578.
- Curran, P.F., Fiore, R.D. & Crisco, J.J. (2008) A comparison of the pressure exerted on soft tissue by 2 myofascial rollers. *J Sport Rehabilitation*, 17, 432–442.
- Federative Committee on Anatomical Terminology. (1998) *Terminologia Anatomica*. Thieme.
- Ferraro, E., Giammarioli, A.M., Chianotto, S., Spoletini, I. & Rosano, G. (2014) Exercise-induced skeletal muscle remodeling and metabolic adaptation: redox signaling and role of autophagy. *Antioxidants & Redox Signaling*, 21, 154–176.
- Franchi, M.V., Reeves, N.D. & Narici, M.V. (2017) Skeletal muscle remodeling in response to eccentric vs. concentric loading: morphological, molecular, and metabolic adaptations. *Frontiers in Physiology*, 8, 447.
- Goh, J. & Ladiges, W. (2015) Voluntary wheel running in mice. *Current Protocols in Mouse Biology*, 5, 283–290.
- Heinle, H. & Lindner, V. (1984) The binding of Evans blue to collagen and elastin in elastic tissue. *Archives Internationales de Physiologie et de Biochimie*, 92, 13–17.
- Hotaling, N.A., Bharti, K., Kriel, H. & Simon, C.G. (2015) DiameterJ: a validated open source nanofiber diameter measurement tool. *Biomaterials*, 61, 327–338.
- Ishihara, A., Hirofujii, C., Nakatani, T., Itoh, K., Itoh, M. & Katsuta, S. (2002) Effects of running exercise with increasing loads on tibialis anterior muscle fibres in mice. *Experimental Physiology*, 87, 113–116.
- Jun, Y.W., Kim, H.R., Reo, Y.J., Dai, M. & Ahn, K.H. (2017) Addressing the autofluorescence issue in deep tissue imaging by two-photon microscopy: the significance of far-red emitting dyes. *Chemical Science*, 8, 7696–7704.
- Kadoguchi, T., Shimada, K., Miyazaki, T., Kitamura, K., Kunimoto, M., Aikawa, T. et al. (2020) Promotion of oxidative stress is associated with mitochondrial dysfunction and muscle atrophy in aging mice. *Geriatrics & Gerontology International*, 20(1), 78–84.
- Kawakami, R., Sawada, K., Kusama, Y., Fang, Y.-C., Kanazawa, S., Kozawa, Y. et al. (2015) In vivo two-photon imaging of mouse hippocampal neurons in dentate gyrus using a light source based on a high-peak power gain-switched laser diode. *Biomedical Optics Express*, 6, 891–901.
- Keeley, F.W., Bellingham, C.M. & Woodhouse, K.A. (2002) Elastin as a self-organizing biomaterial: use of recombinantly expressed human elastin polypeptides as a model for investigations of structure and self-assembly of elastin. *Philosophical Transactions of the Royal Society of London. Series B, Biological sciences*, 357, 185–189.
- Krause, F., Wilke, J., Vogt, L. & Banzer, W. (2016) Intermuscular force transmission along myofascial chains: a systematic review. *Journal of Anatomy*, 228, 910–918.
- Mackey, A.L. & Kjaer, M. (2017) The breaking and making of healthy adult human skeletal muscle in vivo. *Skeletal Muscle*, 7, 24.
- Marieb, E. & Hoehn, K. (2007) *Human anatomy & physiology*. Pearson Education.
- Matsuda, R., Nishikawa, A. & Tanaka, H. (1995) Visualization of dystrophic muscle fibers in mdx mouse by vital staining with Evans blue: evidence of apoptosis in dystrophin-deficient muscle. *Journal of Biochemistry*, 118, 959–964.
- McLoon, L.K., Vicente, A., Fitzpatrick, K.R., Lindström, M. & Pedrosa Domellöf, F. (2018) Composition, architecture, and functional implications of the connective tissue network of the extraocular muscles. *Investigative Ophthalmology & Visual Science*, 59, 322–329.
- Montes, G.S. (1996) Structural biology of the fibres of the collagenous and elastic systems. *Cell Biology International*, 20, 15–27.
- Murphy, C.L. & Lever, M.J. (2002) A ratiometric method of autofluorescence correction used for the quantification of Evans blue dye fluorescence in rabbit arterial tissues. *Experimental Physiology*, 87, 163–170.
- Neubauer, O., Sabapathy, S., Lazarus, R., Jowett, J.B.M., Desbrow, B., Peake, J.M. et al. (2013) Transcriptome analysis of neutrophils after endurance exercise reveals novel signaling mechanisms in the immune response to physiological stress. *Journal of Applied Physiology*, 114, 1677–1688.
- Pasquali-Ronchetti, I., Fornieri, C., Baccarani-Contri, M. & Quaglini, D. (1995) Ultrastructure of elastin. *Ciba Foundation Symposium*, 192, 31–42; discussion 42–50.
- Phillips, D., Rezvani, K. & Bain, B.J. (2000) Exercise induced mobilisation of the marginated granulocyte pool in the investigation of ethnic neutropenia. *Journal of Clinical Pathology*, 53, 481–483.
- Puspoki, Z., Storath, M., Sage, D. & Unser, M. (2016) Transforms and operators for directional bioimage analysis: a survey. *Advances in Anatomy, Embryology and Cell Biology*, 219, 69–93.
- Pyon, W.S., Gray, D.T. & Barnes, C.A. (2019) An alternative to dye-based approaches to remove background autofluorescence from primate brain tissue. *Frontiers in Neuroanatomy*, 13, 73.
- Reed, D.A., Yotsuya, M., Gubareva, P., Toth, P.T. & Bertagna, A. (2019) Two-photon fluorescence and second harmonic generation characterization of extracellular matrix remodeling in post-injury murine temporomandibular joint osteoarthritis. *PLoS One*, 14, e0214072.
- Rezakhaniha, R., Agianniotis, A., Schrauwen, J.T., Griffa, A., Sage, D., Bouten, C. et al. (2012) Experimental investigation of collagen waviness and orientation in the arterial adventitia using confocal laser scanning microscopy. *Biomechanics and Modeling in Mechanobiology*, 11, 461–473.
- Servin-Vences, M.R., Poole, K., Sporbert, A., Lewin, G.R. & Margineanu, A. (2020) Collagen organization within the cartilage of Trpv4(-/-) mice studied with two-photon microscopy and polarized second harmonic generation. *Cytometry A*, 97(5), 504–514.
- Shoji, H. & Miyakawa, T. (2019) Age-related behavioral changes from young to old age in male mice of a C57BL/6J strain maintained under a genetic stability program. *Neuropsychopharmacology Reports*, 39, 100–118.
- Svensson, R.B., Heinemeier, K.M., Coupe, C., Kjaer, M. & Magnusson, S.P. (2016) Effect of aging and exercise on the tendon. *Journal of Applied Physiology*, 121, 1237–1246.
- Theodorakopoulos, C., Jones, J., Bannerman, E. & Greig, C.A. (2017) Effectiveness of nutritional and exercise interventions to improve body composition and muscle strength or function in sarcopenic obese older adults: a systematic review. *Nutrition Research*, 43, 3–15.
- Tozzi, P. (2014) Does fascia hold memories? *Journal of Bodywork and Movement Therapies*, 18, 259–265.
- Tsuchiya, M., Sekiai, S., Hatakeyama, H., Koide, M., Chaweewannakorn, C., Yaoita, F. et al. (2018) Neutrophils provide a favorable IL-1-mediated immunometabolic niche that primes GLUT4 translocation and performance in skeletal muscles. *Cell Reports*, 23, 2354–2364.
- Weizsacker, H.W., Zierler, E. & Juch, H. (2014) A simple method for vital staining of elastin in arterial tissue. *Biomedical Engineering/ Biomedizinische Technik*, 59, 367–373.
- Yanagisawa, H. & Wagenseil, J. (2019) Elastic fibers and biomechanics of the aorta: insights from mouse studies. *Matrix Biology*, 85–86, 160–172.

Zoumi, A., Lu, X., Kassab, G.S. & Tromberg, B.J. (2004) Imaging coronary artery microstructure using second-harmonic and two-photon fluorescence microscopy. *Biophysical Journal*, 87, 2778–2786.

SUPPORTING INFORMATION

Additional supporting information may be found online in the Supporting Information section.

How to cite this article: Chaweewannakorn C, Harada T, Nyasha MR, Koide M, Shikama Y, Hagiwara Y, et al. Imaging of muscle activity-induced morphometric changes in fibril network of myofascia by two-photon microscopy. *J. Anat.* 2021;238:515–526. <https://doi.org/10.1111/joa.13339>